

## **pH dependence of listeriolysin O aggregation and pore-forming ability**

Andrej Bavdek<sup>1,2</sup>, Rok Kostanjšek<sup>1</sup>, Valeria Antonini<sup>3</sup>, Jeremy H. Lakey<sup>4</sup>, Mauro Dalla Serra<sup>3</sup>, Robert J.C. Gilbert<sup>5</sup>, Gregor Anderluh<sup>1,6,\*</sup>

<sup>1</sup> Department of Biology, Biotechnical Faculty, University of Ljubljana, Večna pot 111, 1000 Ljubljana, Slovenia

<sup>2</sup> Present address: INSERM U950, Jacques Monod Institute, University Paris 7, Paris, France

<sup>3</sup> CNR Institute of Biophysics, Unit at Trento and Bruno Kessler Foundation, Via alla Cascata 56/C, 38123 Trento Povo, Italy

<sup>4</sup> University of Newcastle upon Tyne, Framlington Place, Newcastle upon Tyne, NE2 4HH, United Kingdom

<sup>5</sup> Division of Structural Biology, Wellcome Trust Centre for Human Genetics, University of Oxford, Roosevelt Drive, Oxford OX3 7BN, United Kingdom

<sup>6</sup> Present address: National Institut of Chemistry, Hajdrihova 19, 1000 Ljubljana, Slovenia

\* corresponding author: e-mail: gregor.anderluh@ki.si; phone: 00386 1 320 33 97; fax: 00386 1 257 33 90.

Running title: pH dependence of listeriolysin O

Article type : Original Article

Corresponding Author E-mail id: gregor.anderluh@bf.uni-lj.si

This is an Accepted Article that has been peer-reviewed and approved for publication in the *FEBS Journal*, but has yet to undergo copy-editing and proof correction. Please cite this article as an "Accepted Article"; doi: 10.1111/j.1742-4658.2011.08405.x

Abbreviations used: ANS, 1-anilinonaphthalene-8-sulfonic acid; CD, circular dichroism; CDC, cholesterol dependent cytolysins; D1, domain 1; D2, domain 2; D3, domain 3; D4, domain 4; DOPC, 1,2-dioleoyl-*sn*-glycero-3-phosphocholine; LLO, listeriolysin O; PFO, perfringolysin O; PLY, pneumolysin; SLO, streptolysin; TEM, transmission electron microscopy.

## **Summary**

Listeriolysin O (LLO) is the major factor implicated in the escape of *Listeria monocytogenes* from the phagolysosome. It is the only representative of cholesterol dependent cytolysins (CDCs) which exhibits pH dependent activity. Despite intense studies of LLO pH dependence, this feature of the toxin still remains incompletely explained. Here we used fluorescence and circular dichroism spectroscopy to show that LLO structure is not detectably affected by pH at room temperature. We observed slightly altered hemolytic and permeabilising activities at different pH values, which we relate to reduced binding of LLO to the lipid membranes. However, alkaline pH and elevated temperatures causes rapid denaturation of LLO. Aggregates of the toxin are able to bind Congo red and Thioflavin T dyes and are visible under transmission electron microscopy as large, amorphous,  $\mu\text{m}$  sized assemblies. The aggregates have the biophysical properties of amyloid. Analytical ultracentrifugation indicates dimerization of the protein in acidic conditions, which protects the protein against premature denaturation in the phagolysosome, where toxin activity takes place. We therefore suggest that LLO spontaneously aggregates at neutral pH found in the host cell cytosol and that this is a major mechanism of LLO inactivation.

Keywords: cholesterol dependent cytolysin / pore forming toxin / pH dependence / aggregation / permeabilising activity

Subdivision: Membranes

## **Introduction**

The Gram-positive bacterium *Listeria monocytogenes* is a facultative intracellular pathogen. LLO is a major virulence factor, forming pores which allow the escape of *L. monocytogenes* from the phagolysosome and its subsequent replication in the cytosol of host cells during infection [1-3]. The toxin is thus crucial for the intracellular survival of the bacterium [2] and was the first virulence determinant identified in *L. monocytogenes* [4]. LLO is a member of the CDCs, a family of pore forming toxins found predominately in Gram positive bacteria [5,6]. It has the unique property among the CDCs of working optimally at acidic pH. Various studies have revealed a wide variety of effects of LLO on the host cells. It induces calcium release from intracellular (endoplasmic reticulum) stores that leads to cytokine production [7,8], whilst toxin oligomerization on the plasma membrane causes lipid raft aggregation [9,10].

The LLO low pH activity optimum has been observed in several studies. The effect of pH on protein activity was first described by Geoffroy et al. [11]. Unlike other CDCs, such as alveolysin, perfringolysin O (PFO) or pneumolysin (PLY), LLO hemolytic activity on sheep erythrocytes was totally inhibited above pH 7 [11]. The cytolytic activity was maximal at pH ~5.5, which is the pH found in the acidic phagolysosomes. To determine the optimal pH for LLO activity *in vivo*, the lowest pH achieved before perforation was measured for each phagocytic vacuole [12]. Perforation occurred over a range of acidic pH values from 4.9 to

6.7, with a mean near 6.0. LLO also mediated bacterial escape from phagocytic vacuoles and was 10-fold more active at an acidic than neutral pH [13]. Swapping dissimilar residues from a pH-insensitive orthologue PFO identified leucine 461 as responsible for the acidic pH optimum of LLO [14]. Replacement of leucine 461 by the threonine present in PFO increased the hemolytic activity of LLO almost 10-fold at a neutral pH. More recently, Schuerch *et al.* have shown that rapid LLO aggregation at slightly alkaline pH is responsible for LLO inactivation [15], while no reduction in hemolytic activity was detected for PFO under the same conditions. A structural basis for pH-dependant aggregation of LLO was proposed arguing that acidic residues located on  $\alpha$ -helices of domain 3 (D3) determine pH-sensitivity. CDCs are composed of four domains, each of them with a particular role in the pore forming process [5,6,16,17] (Fig. 1a). The initial membrane attachment is achieved by the C-terminal D4 [18]. It is followed by oligomerisation in the plane of the membrane, promoted in part by D1 [19], and significant conformational reorganisation of D3, which results in membrane insertion of two beta hairpins from each monomer [20,21]. The beta hairpins are formed from two bundles of alpha helices of D3. In LLO premature unfurling of these helices to transmembrane hairpins occurs at alkaline pH and temperatures above 33 °C leading to exposure of core hydrophobic residues, normally protected by the D2–D3 interface, to the aqueous milieu [15,22]. Interestingly protein incubation at neutral pH 7 at 37 °C leads to aggregation of only CDCs of listerial origin whereas other representatives such as PFO, streptolysin O (SLO) and PLY retain full haemolytic activity [22].

These recent results are strongly suggestive that the acidic cytolytic activity of LLO is due to a pH-dependent loss of function, not due to pH-dependent activation as had been previously thought. The work of Schuerch and colleagues therefore provides a good foundation for studies of the pH dependence of LLO. Here we report the characterisation of LLO structural

and functional properties in solution at different pH values. We show that, according to fluorescence and circular dichroism (CD) spectroscopy data, LLO structural properties are not directly affected by pH. We have found, however, that the association state of LLO depends markedly upon pH and this suggests a mechanism by which pH and LLO aggregation may be linked. We also show that hemolytic and permeabilising activities are altered by pH values where protein structure is not affected. This is the consequence of the previously observed reduced binding of LLO to lipid membranes [23].

## **Results**

*Properties of LLO in solution* – We have expressed recombinant LLO in *E. coli* and purified it to homogeneity (Fig. 1b). LLO was stable at concentrations below 1 mg/ml and its hemolytic potency was resistant to at least four freeze-thaw cycles. LLO contains one cysteine and we have checked whether our procedures and handling lead to disulphide-linked dimer formation. The amount of dimers was negligible and protein was found to be monomeric on SDS-PAGE analysis (Fig. 1b); there was also no difference in hemolytic activity in the presence or absence of reductant (data not shown).

LLO contains seven tryptophans. One is located in D1, while the rest are in D4 (Fig. 1a) and are, according to the structural model based on the PFO structure [16] (Fig. 1a), mostly exposed to the solvent. The tryptophan emission fluorescence spectra were very similar at pH values between 5.5 and 8.5 and at a temperature of 25 °C (Fig. 1c). The emission maximum was between 345-347 nm. The emission intensity was decreased, and the maximum was shifted to 354 nm, when LLO was denatured with GdnHCl (Fig. 1c). We have also performed tryptophan quenching experiments using potassium iodide. Tryptophans were quenched to the

same degree at all pH values employed and no significant differences between different pH values were observed (inset in Fig. 1c). The fraction of accessible tryptophans ( $f_a$ ) was 0.61-0.71, while effective quenching constant ( $K_{\text{eff}}$ ) was between  $11.6 \pm 2.4$  -  $15.5 \pm 1.5$   $\text{M}^{-1}$  (average  $\pm$  S.D. of 8 independent experiments). The results collectively indicate that the majority of tryptophans are accessible to the solvent and that the pH of the solution does not have profound effects on the environment of the tryptophans.

CD spectra in far and near UV range were measured to obtain additional information on LLO structure at two different pH values. As shown on Fig. 1d spectra recorded at pH 5.5 and 7.5 are very similar with a minimum around 215 nm, characteristic of proteins with high  $\beta$ -structure content. We have determined secondary structure content from the spectra by the use of the Contin algorithm (on DichroWeb server [24]). We found that the secondary structure content was not significantly different between the two used pH values. We determined that recombinant LLO contains  $24.4 \pm 2.4$  and  $20.3 \pm 3.8$  % of alpha-helices,  $25.1 \pm 1.8$  and  $27.5 \pm 3.7$  % of beta-structure,  $20.5 \pm 0.4$  and  $21.8 \pm 0.3$  % of turns and  $30 \pm 0.5$  and  $30.5 \pm 0.2$  % of random structure at pH 5.5 and 7.5, respectively (determined from four independent spectra  $\pm$  S.D.). The near-UV spectra were featureless at both pH values studied when measured at 6  $\mu\text{M}$  LLO concentration (Fig. 1d, inset), in agreement with fluorescence data, which shows that the majority of tryptophans are solvent exposed.

In order to assess the solution state of LLO further, including its oligomerisation, we performed analytical ultracentrifugation (AUC) at pHs 5.5 and 7.5, at 20 °C. LLO behaved in distinctively different ways at the two pHs (Fig. 2a). AUC is particularly well suited to addressing the solution state of LLO because it allows the simultaneous separation of species and assessment of their hydrodynamic properties and weight. The mode of analysis we have

employed (see Materials and methods) allows independent assessment of the number of different species present without assumptions, via the calculation of a  $c(s)$  function. In addition to  $c(s)$  it is possible to calculate the probability of a particular sedimenting species having a range of molecular weights, by computation over a range of theoretical frictional coefficients. The frictional coefficient is a function describing the ratio between the theoretical hydrodynamic behaviour of a protein, given its weight, if it were a sphere and the actual behaviour and hence is an indicator of elongation. A molecular weight can then be calculated for a sedimenting species, taking into account the elongation via the effects of the diffusion coefficient on  $c(s)$  peak breadth; unfolded protein will behave aberrantly however. At pH 5.5 there were three main peaks in the  $c(s)$ , centred on 1.3 S, 3.1 S and 7.0 S. The apparent sedimentation coefficients of individual species in solution can be described by a Gaussian distribution. Deconvolution of these peaks with Gaussians indicated that while the lower two species were each a single sedimenting species, the third peak consisted of two species with  $s = 6.8$  S and 7.2 S. The work of Solovyova and Byron has shown for perfringolysin that the CDC monomer has a sedimentation coefficient of 3.6 S; for pneumolysin it was shown to be the same [25]. These authors also showed the presence of an antiparallel dimer of PFO which has also been observed crystallographically [5,16,26] and which has  $s = 5$  S. Because PLY is not an antiparallel dimer in solution it oligomerises spontaneously in a concentration-dependent manner without the need for cholesterol [25,27,28]. As reported by Solovyova and Byron a parallel dimer (i.e. as found in the structure of the pore [29]) has  $s = 5.4$  S, a trimer 6-7 S, a tetramer  $\sim 8.3$  S etc. On the basis of the foregoing the species observed for LLO at pH 5.5 are most likely a monomer at 3.1 S and a higher molecular weight species with a parallel conformation i.e. a nascent oligomeric state at  $\sim 7.0$  S. The high molecular weight values calculated for the  $\sim 7$  S species supports this conclusion. The ability to deconvolute the  $c(s)$  distribution around 7.0 S in terms of two

Gaussians also makes sense in this case since it would indicate that there are two or more species, being different forms of nascent oligomeric assembly, most likely in dynamic equilibrium as suggested by the breadth of the  $c(s)$  distributions. However, a final insight from the  $c(s)$  profile is that the species at 3.1 S and 7.0 S interconvert rather slowly on the timescale of the experiment since they are well resolved from each other. Although the peak at 1.3 S might appear at first sight to indicate some contaminating material, reference to an SDS-PAGE gel shows that there are no significant species with a lower molecular weight than LLO that might account for it (Fig. 1b). In addition, the peak is absent at pH 7.5 but present at pH 5.5. The presence of this peak can be explained if a proportion of LLO is unfolded at pH 5.5, since unfolded proteins have a much greater hydrodynamic radius ( $R_h$ ) than their folded counterparts of the same weight (and will therefore move much more slowly and appear to be low molecular weight). For example, the desmoglein-specific cytoplasmic region was found to have an experimental  $R_h$  of 41.8 Å against a theoretical value of 24.6 Å for its 28.6 kDa [30]. For this LLO peak, a protein of 55 kDa having  $s=1.3$  S indicates an  $R_h$  of 71.2 Å [31] (the calculated weight for this peak is ~20 kDa). The computed  $R_h$  for monomeric LLO is 35.6 Å using  $s=3.6$  S and the difference observed for the 1.3 S peak shows the unfolded nature of the protein. The percentage contributions of the peaks to the data profile are 21%, 12%, 43% and 27%, respectively. Overall the conclusion for LLO at pH 5.5 is that it is predominately undergoing rapidly interconverting interactions resulting in a complex distribution of apparent sedimentation coefficients in the region of 7 S. At pH 7.5, however, the migration of LLO was very different; instead of well-defined peaks a single, broader  $c(s)$  distribution was observed which, like that around 7 S at pH 5.5 could not be accurately described by a single Gaussian but could be deconvoluted as two Gaussians. One was distributed around a sedimentation coefficient of 2.9 S, similar to the 3.1 S seen for LLO at pH 5.5, and one was distributed around 3.6 S. The merging of these two peaks in a single

overall distribution suggests that they are representative of a rapid interconversion of two different conformations of the LLO monomer. Overall, the results at pH 7.5 indicate metastability in the LLO structure.

To further investigate the relationship between the solution states of LLO and pH we observed the behaviour of the protein as the temperature was raised within the analytical ultracentrifuge (Fig. 2b and c). As the temperature is raised at pH 5.5 the ~7 S peak, visible at 20 °C (Fig. 2a), decreased in amplitude and first larger and then smaller species were visible in an increasingly complex sedimentation profile. This indicates the formation of LLO oligomers in solution, and the stabilisation of the rapidly interconverting interactions seen at 20°C in a series of discrete higher order oligomers. At pH 7.5 the rapidly equilibrating ~7 S peak is absent at a constant 20 °C but as the temperature is raised there is initially an apparent formation of the same well-defined oligomers seen at pH 5.5 but then, when 37 °C is reached, all the higher-order oligomers form a single, broad peak at 11 S.

Structures of the size of LLO can be observed directly using electron microscopy [32]. We have therefore also checked the presence of high-molecular weight aggregates or dimers by transmission electron microscopy (TEM) (Fig. 3). When LLO in buffer with pH 5.5 was deposited on grids and negatively stained, we noted slightly curved ~20 nm long particles, but no larger structures (Fig. 3a). These were visible even if LLO was preincubated for 30 min at 37 °C (Fig. 3b). CDCs are slightly elongated rod-shaped molecules, measuring 115 Å × 30 Å × 55 Å [16]. The observed particles may thus correspond to self-associated aggregates of a couple of LLO molecules and we do not believe they represent nascent, arc-shaped oligomers. We could not observe these particles when LLO was imaged at pH 7.5 below 20 °C. At higher temperatures amorphous aggregates were visible (see below).

The combined results showed that, judging by fluorescence and CD spectroscopy, LLO structure is not affected by pH. LLO is stable below 30 °C and a significant fraction may be found as dimers at pH 5.5. These are not disulfide-linked as shown on an SDS-PAGE gel (Fig. 1b).

*LLO aggregation at different pH values* – Schuerch et al. have shown that LLO aggregates above 33 °C [15]. We have used tryptophan fluorescence, an 1-anilinonaphthalene-8-sulfonic acid (ANS) binding assay and light-scattering to assess aggregation induced by the increase in the temperature at different pH values [15,22]. All three assays showed clear dependence of aggregation on pH. We noted that, for all four pH values studied, changes in tryptophan fluorescence were observed initially (Fig. 4a), then in light scattering and ANS binding (Fig. 4 and Table 1). In agreement with published work [15,22] we found that aggregates were not hemolytically active (see also below) and did not bind to liposomes in an surface plasmon resonance (SPR)- based assay (Fig. 5a). Aggregates are not ordered or fibrillar in structure, but are amorphous  $\mu\text{m}$ -sized structures as revealed by TEM (Fig. 5b) and bright-field microscopy images (Fig. 5c). We have also checked whether aggregated state of LLO at pH 7.5 affect the absorbance and the fluorescence of Congo red and Thioflavine T dyes, respectively, which are routinely used to stain  $\beta$ -sheet amyloid aggregates [33-36]. The LLO aggregates were easily stained in the presence of Congo red and were brightly fluorescent (Fig. 5c). We have observed a characteristic shift in the Congo red absorbance spectrum to approximately 540 nm (solid thick line in Fig. 5d) [33,35]. We have also noted an increase in the Thioflavin T emission maximum in the presence of LLO aggregates (Fig. 5e).

Next we have checked the kinetics of aggregation upon temperature or pH change. First, LLO was incubated in a buffer with pH 5.5 or 7.5 at 20 °C for 15 min. We observed only a slight drift in the signal with time, but not pH-related changes (Fig. 6a), further indicating that protein is stable for a long time at either pH value when kept at temperatures below 30 °C. After the temperature was raised to 37 °C the signal started to change first for tryptophan fluorescence (after approximately 50 s), then for ANS fluorescence (after approximately 100 s) and finally for light scattering (after 200 s). We have also incubated LLO at pH 5.5 and at 37 °C and then changed the pH of the buffer to 7.5 by the addition of small volume of 1 M NaOH (Fig. 6b). Here also the changes in tryptophan fluorescence were noted first and were followed (after 100 s) by the changes in light scattering.

A trypsin cleavage experiment was performed to assess the stability of LLO at two different pH values. At 4 °C there were no differences in susceptibility to trypsin cleavage (Fig. 6c). At both pH values LLO was partially cleaved since some lower molecular weight bands appeared. However, preincubation at 37 °C for 1 h renders LLO extremely sensitive to trypsin digestion, since the protein was cleaved completely at pH 7.5, while at the same temperature at pH 5.5 considerable amounts of uncleaved LLO remained. This experiment is in agreement with the notion that LLO remains stable at temperatures that do not induce aggregation as described above.

*Activity of LLO at different pH values* - Results of others [15,22] and those presented here indicate that pH affects mainly aggregation of LLO above 30 °C in alkaline conditions. In order to check for the effects of pH on the pore-forming ability of LLO, we used hemolytic and planar lipid bilayer assays at around 25 °C, where protein was stable even at pH 7.5.

We have checked the hemolytic activity of LLO preincubated at different temperatures for 30 min at pH 5.5 or 7.5 (Fig. 7a). Preincubation of LLO at higher temperatures (37 and 42 °C) at pH 5.5 resulted in a slight decrease in activity, but even when preincubated at 42 °C there was still significant activity (Fig. 7a). We noted that at pH 7.5 the activity of the protein was significant, when protein was incubated at 4 or 20 °C, but completely lost when incubated at 37 or 42 °C, as expected [15,22] (Fig. 7b). LLO was more active at pH 5.5 when compared to pH 7.5, when activity was assayed at room temperature without prior incubation at any temperature, i.e. used directly from an aliquot kept on ice (Fig. 7c, d). We, however, noted that the kinetics of hemolysis were similar when higher concentrations of LLO were used (Fig. 7c); the protein has a similar lag phase and rate of absorbance decrease.

We also assayed LLO pore forming ability at 24°C in planar lipid membranes (PLM) both at pHs 5.5 and 7.5 (Fig. 8). We used membranes composed of 1,2-dioleoyl-*sn*-glycero-3-phosphocholine (DOPC) with inclusion of 20 or 35 % cholesterol. At both pHs 5.5 and 7.5 LLO is able to destabilize the membrane by forming pores of heterogeneous conductances in the range of pS to nS. Regardless of the pH used, LLO formed lesions that could be clustered into three types of pores, small (conductances below 1 nS), medium (conductances in the range 1-4 nS) and large pores (conductances above 4 nS) (Fig. 8a). However, more pores were observed at pH 5.5 than at 7.5. Events were detected from 25 different experiments (a total of 125 pores at pH 5.5 and 48 pores at pH 7.5). The pore conductivity was spread at both pH values and no pore size difference could be evidenced between the two pH conditions (Fig. 8b). The majority of pores were of small size (59 and 49 % at pH 5.5 and 7.5, respectively), while large pores were rare at both pHs studied (11 and 10 % for pH 5.5 and 7.5, respectively). Cholesterol content directly correlated with LLO activity but it did not

change the pore characteristics. No pore size differences were noted at different cholesterol content (20% or 35%).

The co-presence of slow current increases with unresolved current transitions (small pores) as well as abrupt jumps (big pores) (Fig. 8a), strongly suggesting different pore forming mechanisms and architectures, at least with the lipid composition used. This gradual increase in ionic current has been already described also for other CDCs, like sphaericolysin [37] and pneumolysin [38,39] and for the related human perforin [40] and support a mechanism of coalescence of smaller arcs into larger ones [41].

## **Discussion**

Schuerch et al. provided a good framework to study the pH dependence of LLO [15]. Here we provide further characterisation of LLO structural and functional properties in solution at different pH values. Our results are in accordance with the revised view of LLO pH dependence that LLO is not activated at low pH values, but is rapidly denatured at high pH values [15].

We showed that the tryptophan environment and protein secondary structure is not affected by pH at temperatures that do not promote aggregation and suggest that LLO is stable at acidic pH. Our AUC data indicate that LLO is present in dimeric form at pH 5.5 and is monomeric at pH 7.5. We assume that dimerisation in acidic conditions protects the toxin against oligomerisation and denaturation. The alkaline monomeric form is much more susceptible to denaturation at 37°C according to the fluorescence data. Self-association in solution seems to be a common trait in CDCs. Crystallographic data suggest that PFO forms

head-to-tail dimers in solution [16]. Solovyova *et al.* suggest from AUC and small-angle X-ray scattering data that PFO can be found in solution predominantly as an elongated particle whose shape and volume is consistent with an antiparallel dimer [25]. In contrast to PFO, PLY was detected as a soluble monomer. It was shown that PLY can form oligomers in solution, which are similar to the membrane bound form of the toxin [27,42]. Bourdeau *et al.* determined the anthrolysin O (ALO) structure by X-ray crystallography and found this toxin to be an apparent dimer in the crystal but subsequent characterisation of ALO in solution by sedimentation velocity analysis and SEC coupled to static light scattering revealed this to be a crystallization artifact and that ALO is a monomer in solution [43].

Fluorescence and CD spectroscopy data indicate that at room temperature (25 °C) pH has no effect on listeriolysin conformation and solubility. However, LLO hemolytic activity is dependent on the pH of the buffer at temperatures where protein is stable. The  $c_{50}$  and lag phase are not different, only the concentration needed to achieve similar effects needs to be increased. This would argue that membrane binding is affected and not oligomerisation and that this is underlying reason for the prolongation of the lag phase. We have also checked the ability of LLO to form pores in PLM and show that properties of LLO pores are similar at both pH values. We have also used two different concentrations of cholesterol (20 % or 35 %) and no pore size differences were present. We have previously shown that LLO is able to efficiently permeabilise model lipid membranes and cells at physiological and slightly basic pHs when the cholesterol concentration in the membranes was high [23]. We have also shown that binding is considerably affected by pH at a given cholesterol concentration, when measured at temperatures that do not promote aggregation, i.e. 25 °C (see Fig. 1 in [23]). In summary, all these results show that the membrane binding of LLO is affected by pH, but not the mechanism of pore formation, which proceeds through the same steps.

LLO is secreted into the host cell cytosol and is degraded by the proteasome [44,45]. The fate of LLO in the cytosol is affected by the 26-amino-acid PEST sequence located at the end of N-terminus [46]. PEST sequences serve as a degradation tag for rapid protein degradation in eukaryotic cells. In LLO, three amino acid residues at positions Ser44, Ser48 and Thr51 can be targets of phosphorylation in the host cell cytosol, which is followed by ubiquitinylation and degradation in proteasomes. Potential phosphorylation sites located within LLO's PEST-like sequence are therefore important for compartmentalization of LLO activity and for virulence [44]. Inhibition of proteasomal activity or LLO mutants with extended half-lives are not cytotoxic, which suggests some other mechanisms for preventing full activity in the host cell cytosol [47]. Formation of ubiquitinated protein aggregates infected by *L. monocytogenes* was very frequent and 83% of infected cells showed multiple ubiquitin aggregates. The most recent published investigations reveal the degradation of the toxin at the proteasome complexes within 15 minutes after *Listeria* enter the cytosol [44]. We characterised the aggregation by several means and we show that it is fast, on a seconds-minutes scale, and irreversible. Bright-field microscopy and TEM micrographs display unstructured aggregates up to 5  $\mu\text{m}$  in size when LLO is preincubated at pH 7.5 on 37 °C: This resembles the size of ubiquitinated aggregates observed by immunofluorescence in the cytosol of mammalian cells. It was thus suggested that LLO can form ordered aggregates similar to aggregates of proteins of some neurodegenerative diseases [47]. In contrast our study reveals that aggregates are amorphous structures and not globally ordered ones such as fibrils (Fig. 5). The binding of dyes Congo red and Thioflavin T that are usually used to detect  $\beta$ -sheet rich structures of amyloid fibrils is indicative that at least some  $\beta$ -sheet structures are present in LLO aggregates, and thus that there is an underlying fibrous structure despite the amorphous appearance of the aggregates. This was further corroborated by Tango software calculations

(<http://tango.crg.es/>) [48] for prediction of aggregating regions in unfolded polypeptide chains, which indicate that LLO exhibits some, but a low tendency for  $\beta$ -aggregation. For example with input parameters of 37 °C, 0.15 M salt concentration and pH 5.5 or 7.5, respectively, LLO is predicted to have less than 10 % tendency, while maximal tendency was 20 % at 4 °C regardless of pH. Referenced papers for amyloid proteins indicated that this value is between 50-100 % [35,49,50]. The results from software prediction are thus in agreement with bright-field microscopy and TEM micrographs and indicate that LLO do not have high tendency to form ordered  $\beta$ -sheet aggregates such as proteins involved in neurodegenerative diseases, but that these structures can be formed when the protein is denatured. These data are in agreement with a consensus that all proteins can, if denatured, be induced to form amyloid-like aggregates [34]. The CDCs have a prominent, C-terminal immunoglobulin superfamily domain which may be the basis for their aggregation into amyloid-like structures; such folds are notoriously prone to amyloidogenesis [27,34].

In this study we show that LLO adopts a monomeric state at neutral pH and 25 °C. The toxin rapidly aggregates once the temperature is raised to 37°C. In these conditions which resemble the host cell cytosol, LLO is thus found in an unstructured aggregate form, unable to bind membrane cholesterol, unable to form pores and therefore cytolytically inactive. Since this aggregation is much faster than ubiquitinylation and proteosomal degradation we suspect it to be the major mechanism for inactivation of the toxin. At acidic pH and 37 °C, conditions which resemble the phagolysosome, LLO is found in dimeric form. We suggest that dimerization in acidic conditions is the main feature that protects LLO against aggregation and therefore inactivation.

## Materials and methods

*Cloning, expression and purification of LLO* - The coding region for LLO without signal sequence was amplified by PCR using oligonucleotides LLO+ (5'-CGCGGATCCAAGGATGCATCTGCATTC-3') and LLO- (5'-CGCGGATCCACGCGTTTATTCGATTGGATTATCTACTTTATTAC-3'). The PCR product was cleaved with *Bam*HI and *Mlu*I, and inserted into a precleaved T7-promoter-based expression vector. A modified version of pET8c vector was used that leaves a His<sub>6</sub>-tag with a thrombin recognition sequence at the N-terminal to allow for easier purification [51]. The correct construction of the plasmid was verified by nucleotide sequencing. LLO was expressed in an *Escherichia coli* BL21(DE3)pLysS strain (Novagen). Overnight culture (50 ml) was used to inoculate 3 l of Luria–Bertani medium with 100 µg/ml ampicillin. Expression of LLO was induced at an A<sub>600</sub> of approx. 0.8 by the addition of isopropyl β-D-thiogalactoside at a final concentration of 0.5 mM. Cells were grown for an additional 5 h at 30 °C, centrifuged at 2800 g for 20 min at 4 °C and frozen at –20 °C. From the frozen cells, 8 g were thawed into 20 ml of 50 mM sodium phosphate buffer (pH 6.5), 300 mM NaCl, 20 mM 2-mercaptoethanol, 1 mg/ml lysozyme, 10 µg/ml DNase, 20 µg/ml RNase, 0.5 mM PMSF, 0.5 mM AEBSF and 1 mM benzamidine. They were incubated on ice for 45 min with occasional vigorous shaking. Bacteria were sonicated for 4 × 2 min during the incubation by using a microtip of Sonics VCX 750W ultrasonic disintegrator. Broken cells were centrifuged for 30 min at 4 °C at 11000 g (Sigma). The supernatants were applied to a 2 ml Ni-NTA (nitrilotriacetate) column (Qiagen, Crawley, U.K.), which had been equilibrated with 50 mM sodium phosphate buffer (pH 6.5), 10 mM imidazole. Unbound proteins were eluted with the above buffer and the bound LLO was eluted by 50 mM NaH<sub>2</sub>PO<sub>4</sub>, pH 7.0, 300 mM imidazole. The protein was dialysed three times against 2 l of 15 mM NaH<sub>2</sub>PO<sub>4</sub>, 150 mM NaCl, 0.001 M

EDTA, pH 5.7 at 4 °C. Ion-exchange chromatography on an Äkta™ FPLC system (Amersham Biosciences) was used as a final purification step. The sample was applied to a MonoS column equilibrated with 0.015 M NaH<sub>2</sub>PO<sub>4</sub>, 0.15 M NaCl, pH 5.7 and bound LLO was eluted from the column by a gradient of the same buffer with 1 M NaCl. Fractions shown to contain LLO by SDS/PAGE (12% gels), were merged and stored at -20 °C. Molar absorption coefficient for His-tagged LLO,  $\epsilon^{0.1\%}$  (for 1 g/l of protein solution), calculated from the sequence at ExPASy Proteomics tools Internet site (<http://us.expasy.org/tools/>) was 1.315.

*Fluorescence measurements* - All fluorescence measurements were performed on a Jasco FP-750 spectrofluorimeter (Jasco Corporation, Japan). The sample compartment was equipped with a Peltier thermostatted single cell holder. Steady-state tryptophan spectra were measured at 25 °C with constant stirring. Excitation wavelength was fixed at 295 nm, to eliminate the contribution of the tyrosines, and the emission spectra were recorded between 310 and 400 nm. Excitation and emission slits were set at 5 nm. Protein concentration in the cuvette was 250 nM in a final volume of 1200  $\mu$ l. Buffers were MES, pH 5.5 (20mM NaH<sub>2</sub>PO<sub>4</sub>, 140 mM NaCl, 1 mM EDTA), phosphate, pH 6.5 (20mM MES, 140 mM NaCl, 1 mM EDTA) and Hepes, pH 7.5 and 8.5 (20mM Hepes, 140 mM NaCl, 1 mM EDTA).

For the iodide quenching experiments the concentration of LLO was 250 nM in the above buffers. Spectra were recorded without and in the presence of increasing iodide concentrations. The stock of iodide was composed of 2.5 M KI and 0.001 M Na<sub>2</sub>S<sub>2</sub>O<sub>3</sub>. All spectra were corrected with the corresponding spectra of the buffer alone and for the dilution caused by the addition of iodide. No further correction for wavelength-dependent sensitivity

was done. The values of the collisional effective quenching constant were obtained from the Stern–Volmer equation modified for multiple emission centres [52]:

$$F_0/(F_0 - F) = (1/f_a \times K_{\text{eff}}) \times 1/Q + 1/f_a \quad (\text{eq. 1})$$

where  $F_0$  is the fluorescence intensity in the absence of iodide,  $F$  is the fluorescence intensity in the presence of iodide,  $f_a$  is the fraction of accessible tryptophans,  $K_{\text{eff}}$  is the effective quenching constant and  $Q$  is iodide concentration.

*Light scattering* – Light scattering data were obtained by Jasco FP-750 spectrofluorimeter, similar to fluorescence measurements. Scattering intensity was followed at excitation and emission wavelengths set to 600 nm. Measurements were taken between 15 and 70 °C at heating rate 1 °C/min and constant stirring. Protein concentration in the cuvette was 250 nM in a final volume of 1200 µl. The same buffer solutions as for fluorescence measurement were used.

*Circular dichroism spectroscopy* - CD spectra were measured by Jasco J-810 spectropolarimeter. Bandwidth was set to 2 nm; scanning speed was 20 nm/min. The protein concentration in 20 mM sodium phosphate buffer (pH 5.5 and 7.5), was 6 µM. A 0.02 cm pathlength cuvette was used for far-UV and 0.5 cm pathlength cuvette for near-UV CD spectra measurements, respectively. Spectra were scanned from 250–185 nm in the far-UV CD region and from 320–250 in near-UV CD region at 20 °C. The reported spectra are averages of 10 scans.

*Analytical ultracentrifugation* - Analytical ultracentrifugation experiments were performed using a Beckman Optima XL-I centrifuge in sedimentation velocity mode. The samples were held in 12 mm Epon sector-shaped 2-channel centrepieces and were spun at 40,000 rpm, with

50 sample distribution scans being taken increments of 4 minutes apart and data being collected using 280 nm absorbance and interference optics, analysed using Sedfit [53,54]. Size-and-shape distribution ( $c(s,f_r)$ ) analysis was used, where  $f_r$  is the frictional ratio and a sphere has a frictional ratio of 1 and other species of  $>1$ . This allows the plotting of contour plots of  $c(s,M)$  where  $M$  is the weight of the protein. A critical parameter in analysis of this kind is the limiting  $f_r$  and we performed it with a range of values from 1-2, non-trivial peaks in the  $c(s,M)$  function being successfully found within the boundaries of the calculation. The % area represented by each Gaussian species was calculated using the equation:

$$A = \sigma\alpha\sqrt{2\pi} \quad (\text{eq. 2})$$

where  $A$  is the area,  $\sigma$  the half width, and  $\alpha$  the height of each peak [55].

*Transmission electron microscopy* - LLO at concentration 0.25  $\mu\text{M}$  in 20 mM  $\text{NaH}_2\text{PO}_4$ , 0.14 M NaCl, pH 5.5 or 7.5 was incubated for 30 min at 37  $^\circ\text{C}$ . 10  $\mu\text{l}$  of protein preparation were transferred on copper grid. After removal of excessive suspension by filter paper, samples were stained with 0.1% (m:v) aqueous solution of uranyl acetate, which was filtered out after 2 seconds. Samples were air dried and before observation with a Philips CM 100 transmission electron microscope operating at 80 kV.

*ANS binding assay* - The fluorescence of ANS in the presence of LLO was followed from 420-550 nm with excitation wavelength set to 370 nm. Excitation and emission slits were set to 5 nm. The cuvette was placed in a thermostatted cell holder, and the contents were stirred continuously. Measurements were taken between 15 and 75  $^\circ\text{C}$  by using a 1  $^\circ\text{C}/\text{min}$  heating rate. The concentration of ANS and protein was 15 and 1  $\mu\text{M}$ , respectively.

*Surface plasmon resonance* - SPR measurements were performed on a Biacore T100 (GE Healthcare, Biacore AB, Uppsala, Sweden) apparatus at 25 °C. An L1 chip was equilibrated in 20 mM Tris-HCl, 140 mM NaCl, and 1 mM EDTA, pH 6.5. Large unilamellar vesicles of 100 nm diameter were prepared by extrusion as described [56,57]. Liposomes were composed of 1,2-dioleoyl-*sn*-glycero-3-phosphocholine (DOPC) and cholesterol at 60:40 ratio (mol:mol). The liposome-coated chip surface was prepared as described by Anderluh *et al.* [56]. LLO was preincubated at various pH and temperature 4 and 37 °C for 30 min. Preincubated LLO was injected over these prepared surfaces at the desired concentration for 90 s at a flow rate of 30 µL/min and the dissociation was followed for 3 min. Blank injections were subtracted from sensorgrams to correct for the contribution of buffer and DTT to the increase of the response.

*Congo red and Thioflavin T spectroscopic measurements* – Experiments were performed in 20 mM Tris-HCl, 150 mM NaCl, pH 7.5. The concentration of Congo red was approximately 20 µM. The absorbance spectra were recorded in the absence or presence of 2 µM aggregated LLO between 400 and 600 nm in a 1 cm pathlength cuvette by UV-2101 PC spectrophotometer (Shimadzu). The Thioflavin T fluorescence was excited at 440 nm and the emission spectra were recorded between 455-600 nm. The final concentrations of Thioflavin T and LLO were 20 and 2.5 µM, respectively. Other conditions were as described above.

*Trypsin digestion experiment* – Five micrograms of LLO were incubated for 1 h at 4 or 37 °C in pH 5.5 or 7.5 buffer. Then trypsin was added to a LLO:trypsin ratio 1:60 or 1:100 (w:w) and incubated overnight at 22 °C. Proteins were then precipitated with 10 % of trichloroacetic acid, resuspended in SDS-PAGE loading buffer and resolved on 12 % SDS-PAGE gels. Gels were stained with Coomassie-blue.

*Haemolytic activity* - Haemolytic activity was measured in terms of attenuation on human erythrocytes at 20 °C using a microplate reader (MRX; Dynex Technologies, Denkendorf, Germany). LLO at concentration 10 nM LLO was added in the first well to erythrocyte buffer (0.15 M NaCl, 0.02 NaH<sub>2</sub>PO<sub>4</sub>, 1 mM EDTA, pH 5.5 or 7.5), and then serially diluted 2-fold. Human erythrocytes (100 µl ; A<sub>630</sub>=0.5) in erythrocyte buffer were added to the toxin, and haemolysis was monitored by measuring attenuation at 630 nm for 20 min at room temperature. The final volume in all wells was 200 µl.

*Planar lipid membranes* - PLM were prepared by the apposition techniques as described in Dalla Serra and Menestrina [58]: two monolayers were spread from a 5 mg/ml lipid solution in pentane on the top of 2 ml chambers made of Teflon. Normally a mixture comprised of DOPC:cholesterol 80:20 or 65:35 (mol:mol) was used. The septum between the chambers was made of 25 µm thick teflon film and contained a 160 µm hole. LLO was added at 10-20 nM concentrations to stable, preformed bilayers on one side only (called the cis side where the electrical potential was applied, the trans side being grounded). Typically, untreated membranes had a capacitance of 115 pF and a conductance not exceeding 10 pS. Voltage clamp experiments were conducted using a Axon patch clamp amplifier (Axopatch 200, Axon Instruments, Foster City, CA). A PC equipped with a DigiData 1200 A/D converter (Axon Instruments) was used for data acquisition. The current was filtered at 0.5 kHz and acquired at 2 kHz by the computer using Axoscope 8 software (Axon Instruments). Ag-AgCl electrodes were connected to the electrolyte solution via agarose bridges saturated with 3 M KCl. The bathing solutions contained KCl 100 mM and 10 mM MES or Hepes at pH 5.5 or 7.5 respectively. Experiments were performed at 24°C.

The current across the bilayer was measured, and the conductance (G) was determined as follows:

$$G \text{ (nS)} = I \text{ (pA)} / V \text{ (mV)}, \quad (\text{eq. 3})$$

where I is the current through the membrane, and V is the applied transmembrane potential.

The radius of LLO pores were estimated according to:

$$r = [(GL) / (\pi\sigma)]^{1/2} \quad (\text{eq. 4})$$

where r is the pore radius,  $\sigma$  is the conductivity of the solution (12 mS/cm in our case), L is the length of the pore (estimated to be 20 nm) and G its conductance.

### **Acknowledgments**

We would like to thank the anonymous referees for the suggestion to use the TANGO software and other useful comments and suggestions. The work in this study was supported by "Toxins and biomembranes" Programme grant and J1-9591 project of the Slovenian Research Agency, Italy-Slovenia bilateral project "Pore-forming toxins as useful tools in biotechnology-molecular mechanisms of action" and Nanosmart project from Provincia Autonoma di Trento. RJCG is a Royal Society University Research Fellow.

## References:

- [1] Gaillard JL, Berche P, Mounier J, Richard S & Sansonetti P (1987) In vitro model of penetration and intracellular growth of *Listeria monocytogenes* in the human enterocyte-like cell line Caco-2. *Infect Immun* **55**, 2822-2829.
- [2] Portnoy DA, Jacks PS & Hinrichs DJ (1988) Role of Hemolysin for the Intracellular Growth of *Listeria-Monocytogenes*. *J Exp Med* **167**, 1459-1471.
- [3] Cossart P, Vicente MF, Mengaud J, Baquero F, Perez-Diaz JC & Berche P (1989) Listeriolysin O is essential for virulence of *Listeria monocytogenes*: direct evidence obtained by gene complementation. *Infect Immun* **57**, 3629-3636.
- [4] Girard KF, Sbarra AJ & Bardawil WA (1963) Serology of *Listeria monocytogenes*. I. Characteristics of the soluble hemolysin. *J Bacteriol* **85**, 349-355.
- [5] Gilbert RJ (2005) Inactivation and activity of cholesterol-dependent cytolysins: what structural studies tell us. *Structure*. **13**, 1097-1106.
- [6] Tweten RK (2005) Cholesterol-dependent cytolysins, a family of versatile pore-forming toxins. *Infect Immun* **73**, 6199-6209.
- [7] Gekara NO, Westphal K, Ma B, Rohde M, Groebe L & Weiss S (2007) The multiple mechanisms of Ca<sup>2+</sup> signalling by listeriolysin O, the cholesterol-dependent cytolysin of *Listeria monocytogenes*. *Cell Microbiol* **9**, 2008-2021.
- [8] Gekara NO, Groebe L, Viegas N & Weiss S (2008) *Listeria monocytogenes* Desensitizes Immune Cells to Subsequent Ca<sup>2+</sup> Signaling via Listeriolysin O-Induced Depletion of Intracellular Ca<sup>2+</sup> Stores. *Infect Immun* **76**, 857-862.
- [9] Gekara NO & Weiss S (2004) Lipid rafts clustering and signalling by listeriolysin O. *Biochem Soc Trans* **32**, 712-714.

- [10] Gekara NO, Jacobs T, Chakraborty T & Weiss S (2005) The cholesterol-dependent cytolysin listeriolysin O aggregates rafts via oligomerization. *Cell Microbiol* **7**, 1345-1356.
- [11] Geoffroy C, Gaillard JL, Alouf JE & Berche P (1987) Purification, characterization, and toxicity of the sulfhydryl-activated hemolysin listeriolysin O from *Listeria monocytogenes*. *Infect Immun* **55**, 1641-1646.
- [12] Beauregard KE, Lee KD, Collier RJ & Swanson JA (1997) pH-dependent perforation of macrophage phagosomes by listeriolysin O from *Listeria monocytogenes*. *J Exp Med* **186**, 1159-1163.
- [13] Glomski IJ, Gedde MM, Tsang AW, Swanson JA & Portnoy DA (2002) The *Listeria monocytogenes* hemolysin has an acidic pH optimum to compartmentalize activity and prevent damage to infected host cells. *J Cell Biol* **156**, 1029-1038.
- [14] Glomski IJ, Decatur AL & Portnoy DA (2003) *Listeria monocytogenes* Mutants That Fail To Compartmentalize Listeriolysin O Activity Are Cytotoxic, Avirulent, and Unable To Evade Host Extracellular Defenses. *Infect Immun* **71**, 6754-6765.
- [15] Schuerch DW, Wilson-Kubalek EM & Tweten RK (2005) Molecular basis of listeriolysin O pH dependence. *Proc Natl Acad Sci USA* **102**, 12537-12542.
- [16] Rossjohn J, Feil SC, McKinsty WJ, Tweten RK & Parker MW (1997) Structure of a cholesterol-binding, thiol-activated cytolysin and a model of its membrane form. *Cell* **89**, 685-692.
- [17] Anderluh G & Lakey JH (2008) Disparate proteins use similar architectures to damage membranes. *Trends Biochem Sci* **33**, 482-490.
- [18] Ramachandran R, Heuck AP, Tweten RK & Johnson AE (2002) Structural insights into the membrane-anchoring mechanism of a cholesterol-dependent cytolysin. *Nat Struct Biol* **9**, 823-827.

- [19] Ramachandran R, Tweten RK & Johnson AE (2005) The domains of a cholesterol-dependent cytolysin undergo a major FRET-detected rearrangement during pore formation. *Proc Natl Acad Sci USA* **102**, 7139-7144.
- [20] Shepard LA, Heuck AP, Hamman BD, Rossjohn J, Parker MW, Ryan KR, Johnson AE & Tweten RK (1998) Identification of a membrane-spanning domain of the thiol-activated pore-forming toxin *Clostridium perfringens* perfringolysin O: an alpha-helical to beta-sheet transition identified by fluorescence spectroscopy. *Biochemistry* **37**, 14563-14574.
- [21] Shatursky O, Heuck AP, Shepard LA, Rossjohn J, Parker MW, Johnson AE & Tweten RK (1999) The mechanism of membrane insertion for a cholesterol-dependent cytolysin: a novel paradigm for pore-forming toxins. *Cell* **99**, 293-299.
- [22] Nomura T, Kawamura I, Kohda C, Baba H, Ito Y, Kimoto T, Watanabe I & Mitsuyama M (2007) Irreversible loss of membrane-binding activity of *Listeria*-derived cytolysins in non-acidic conditions: a distinct difference from allied cytolysins produced by other Gram-positive bacteria. *Microbiology* **153**, 2250-2258.
- [23] Bavdek A, Gekara NO, Priselac D, Gutierrez Aguirre I, Darji A, Chakraborty T, Maček P, Lakey JH, Weiss S & Anderluh G (2007) Sterol and pH interdependence in the binding, oligomerization, and pore formation of Listeriolysin O. *Biochemistry* **46**, 4425-4437.
- [24] Whitmore L & Wallace BA (2008) Protein secondary structure analyses from circular dichroism spectroscopy: methods and reference databases. *Biopolymers* **89**, 392-400.
- [25] Solovyova AS, Nollmann M, Mitchell TJ & Byron O (2004) The Solution Structure and Oligomerization Behavior of Two Bacterial Toxins: Pneumolysin and Perfringolysin O. *Biophys J* **87**, 540-552.
- [26] Rossjohn J, Polekhina G, Feil SC, Morton CJ, Tweten RK & Parker MW (2007) Structures of perfringolysin O suggest a pathway for activation of cholesterol-dependent cytolysins. *J Mol Biol* **367**, 1227-1236.

- [27] Gilbert RJC, Rossjohn J, Parker MW, Tweten RK, Morgan PJ, Mitchell TJ, Errington N, Rowe AJ, Andrew PW & Byron O (1998) Self-interaction of pneumolysin, the pore-forming protein toxin of *Streptococcus pneumoniae*. *J Mol Biol* **284**, 1223-1237.
- [28] Gilbert RJ, Jimenez JL, Chen S, Tickle IJ, Rossjohn J, Parker M, Andrew PW & Saibil HR (1999) Two structural transitions in membrane pore formation by pneumolysin, the pore-forming toxin of *Streptococcus pneumoniae*. *Cell* **97**, 647-655.
- [29] Tilley SJ, Orlova EV, Gilbert RJ, Andrew PW & Saibil HR (2005) Structural basis of pore formation by the bacterial toxin pneumolysin. *Cell* **121**, 247-256.
- [30] Kami K, Chidgey M, Dafforn T & Overduin M (2009) The desmoglein-specific cytoplasmic region is intrinsically disordered in solution and interacts with multiple desmosomal protein partners. *J Mol Biol* **386**, 531-543.
- [31] Uversky VN (1993) Use of fast protein size-exclusion liquid chromatography to study the unfolding of proteins which denature through the molten globule. *Biochemistry* **32**, 13288-13298.
- [32] Law RH, Lukyanova N, Voskoboinik I, Caradoc-Davies TT, Baran K, Dunstone MA, D'Angelo ME, Orlova EV, Coulibaly F, Verschoor S, Browne KA, Ciccone A, Kuiper MJ, Bird PI, Trapani JA, Saibil HR, Whisstock J (2010) The structural basis for membrane binding and pore formation by lymphocyte perforin. *Nature* **468**, 447-451.
- [33] Žerovnik E, Pompe-Novak M, Škarabot M, Ravnikar M, Muševič I & Turk V (2002) Human stefin B readily forms amyloid fibrils in vitro. *Biochim Biophys Acta* **1594**, 1-5.
- [34] Wright CF, Teichmann SA, Clarke J & Dobson CM (2005) The importance of sequence diversity in the aggregation and evolution of proteins. *Nature* **438**, 878-881.
- [35] Ramsook CB, Tan C, Garcia MC, Fung R, Soybelman G, Henry R, Litewka A, O'Meally S, Otoo HN, Khalaf RA, Dranginis AM, Gaur NK, Klotz SA, Rauceo JM, Jue CK & Lipke

PN (2010) Yeast cell adhesion molecules have functional amyloid-forming sequences. *Eukaryot Cell* **9**, 393-404.

[36] Sonnen AF, Yu C, Evans EJ, Stuart DI, Davis SJ & Gilbert RJ (2010) Domain metastability: a molecular basis for immunoglobulin deposition? *J Mol Biol* **399**, 207-213.

[37] From C, Granum PE & Hardy SP (2008) Demonstration of a cholesterol-dependent cytolysin in a noninsecticidal *Bacillus sphaericus* strain and evidence for widespread distribution of the toxin within the species. *FEMS Microbiol Lett* **286**, 85-92.

[38] Korchev YE, Bashford CL & Pasternak CA (1992) Differential sensitivity of pneumolysin-induced channels to gating by divalent cations. *J Membr Biol* **127**, 195-203.

[39] El-Rachkidy RG, Davies NW & Andrew PW (2008) Pneumolysin generates multiple conductance pores in the membrane of nucleated cells. *Biochem Biophys Res Commun* **368**, 786-792.

[40] Praper T, Sonnen A, Viero G, Kladnik A, Froelich CJ, Anderluh G, Dalla Serra M & Gilbert RJ (2011) Human perforin employs different avenues to damage membranes. *J Biol Chem* **286**, 2946-2955.

[41] Palmer M, Vulicevic I, Saweljew P, Valeva A, Kehoe M & Bhakdi S (1998) Streptolysin O: A Proposed Model of Allosteric Interaction between a Pore-Forming Protein and Its Target Lipid Bilayer. *Biochemistry* **37**, 2378-2383.

[42] Gilbert RJC, Heenan RK, Timmins PA, Gingles NA, Mitchell TJ, Rowe AJ, Rossjohn J, Parker MW, Andrew PW & Byron O (1999) Studies on the structure and mechanism of a bacterial protein toxin by analytical ultracentrifugation and small-angle neutron scattering. *J Mol Biol* **293**, 1145-1160.

[43] Bourdeau RW, Malito E, Chenal A, Bishop BL, Musch MW, Villereal ML, Chang EB, Mosser EM, Rest RF & Tang WJ (2009) Cellular functions and X-ray structure of anthrolysin

O, a cholesterol-dependent cytolysin secreted by *Bacillus anthracis*. *J Biol Chem* **284**, 14645-14656.

[44] Schnupf P, Portnoy DA & Decatur AL (2006) Phosphorylation, ubiquitination and degradation of listeriolysin O in mammalian cells: role of the PEST-like sequence. *Cell Microbiol* **8**, 353-364.

[45] Schnupf P, Zhou J, Varshavsky A & Portnoy DA (2007) Listeriolysin O Secreted by *Listeria monocytogenes* into the Host Cell Cytosol Is Degraded by the N-End Rule Pathway. *Infect Immun* **75**, 5135-5147.

[46] Rogers S, Wells R & Rechsteiner M (1986) Amino acid sequences common to rapidly degraded proteins: the PEST hypothesis. *Science* **234**, 364-368.

[47] Viala JP, Mochegova SN, Meyer-Morse N & Portnoy DA (2008) A bacterial pore-forming toxin forms aggregates in cells that resemble those associated with neurodegenerative diseases. *Cell Microbiol* **10**, 985-993.

[48] Fernandez-Escamilla AM, Rousseau F, Schymkowitz J & Serrano L (2004) Prediction of sequence-dependent and mutational effects on the aggregation of peptides and proteins. *Nat Biotechnol* **22**, 1302-1306.

[49] Linding R, Schymkowitz J, Rousseau F, Diella F & Serrano L (2004) A comparative study of the relationship between protein structure and beta-aggregation in globular and intrinsically disordered proteins. *J Mol Biol* **342**, 345-353.

[50] Rousseau F, Schymkowitz J & Serrano L (2006) Protein aggregation and amyloidosis: confusion of the kinds? *Curr Opin Struct Biol* **16**, 118-126.

[51] Kristan K, Viero G, Maček P, Dalla Serra M & Anderluh G (2007) The equinatoxin N-terminus is transferred across planar lipid membranes and helps to stabilize the transmembrane pore. *FEBS J* **274**, 539-550.

- [52] Eftink MR & Ghiron CA (1981) Fluorescence quenching studies with proteins. *Anal Biochem* **114**, 199-227.
- [53] Schuck P & Rossmanith P (2000) Determination of the sedimentation coefficient distribution by least-squares boundary modeling. *Biopolymers* **54**, 328-341.
- [54] Brown PH & Schuck P (2006) Macromolecular size-and-shape distributions by sedimentation velocity analytical ultracentrifugation. *Biophys J* **90**, 4651-4661.
- [55] Harkiolaki M, Gilbert RJ, Jones EY & Feller SM (2006) The C-terminal SH3 domain of CRKL as a dynamic dimerization module transiently exposing a nuclear export signal. *Structure*. **14**, 1741-1753.
- [56] Anderluh G, Beseničar M, Kladnik A, Lakey JH & Maček P (2005) Properties of nonfused liposomes immobilized on an L1 Biacore chip and their permeabilization by a eukaryotic pore-forming toxin. *Anal Biochem* **344**, 43-52.
- [57] Beseničar M, Maček P, Lakey JH & Anderluh G (2006) Surface plasmon resonance in protein-membrane interactions. *Chem Phys Lipids* **141**, 169-178.
- [58] Dalla Serra M & Menestrina G (2000) Characterization of molecular properties of pore-forming toxins with planar lipid bilayers. *Methods Mol Biol* **145**, 171-188.

## Tables

**Table 1: Summary of LLO aggregation as measured by different approaches**

	Start of increase in signal intensity (°C)			
	pH 5.5	pH 6.5	pH 7.5	pH 8.5
<b>Trp fluorescence</b> (n=8)	30	35	40	40
<b>Light scattering</b> (n=7)	35	37.5	41.5	44.5
<b>ANS fluorescence</b> (n=5)	40	40	45	45

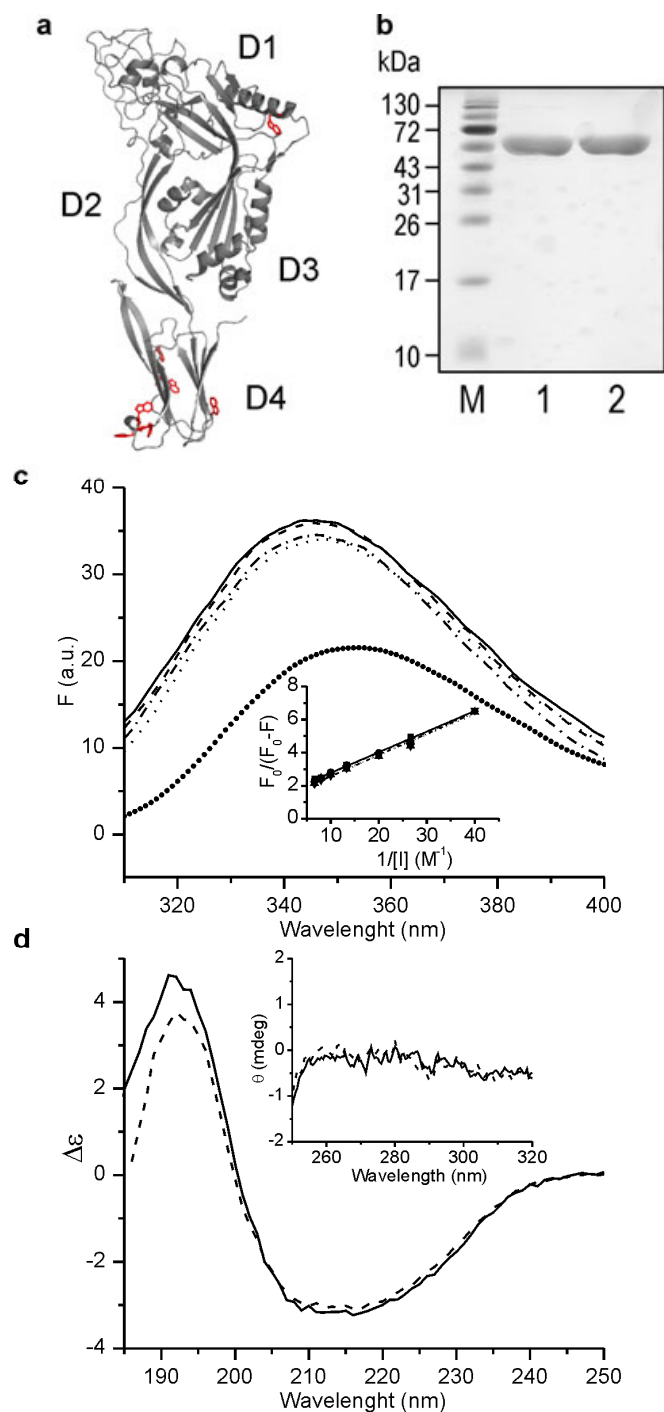


**Figure 1: Properties of LLO in solution**

(a) LLO model with Trps side chains shown in red and its four domains denoted D1-D4. (b) Five  $\mu\text{g}$  of LLO were resolved on 12% SDS-PAGE gel and stained with Coomassie blue under non-reducing (1) or reducing (2) conditions. M, marker. (c) Trp fluorescence spectra of

250 nM LLO at four different pH values at 25 °C. Solid line, pH 5.5; dashed line, pH 6.5, dotted line, pH 7.5; dash-dotted line, pH 8.5. The spectra in the presence of denaturant 6 M GdnHCl is shown by circles. Inset, iodide quenching data for four different pH values. The designations of the lines is the same as above. (d) Far- UV CD spectra of LLO at pH 5.5 (solid line) and 7.5 (dashed line). The inset shows near-UV CD spectra of LLO at pH 5.5 and 7.5.

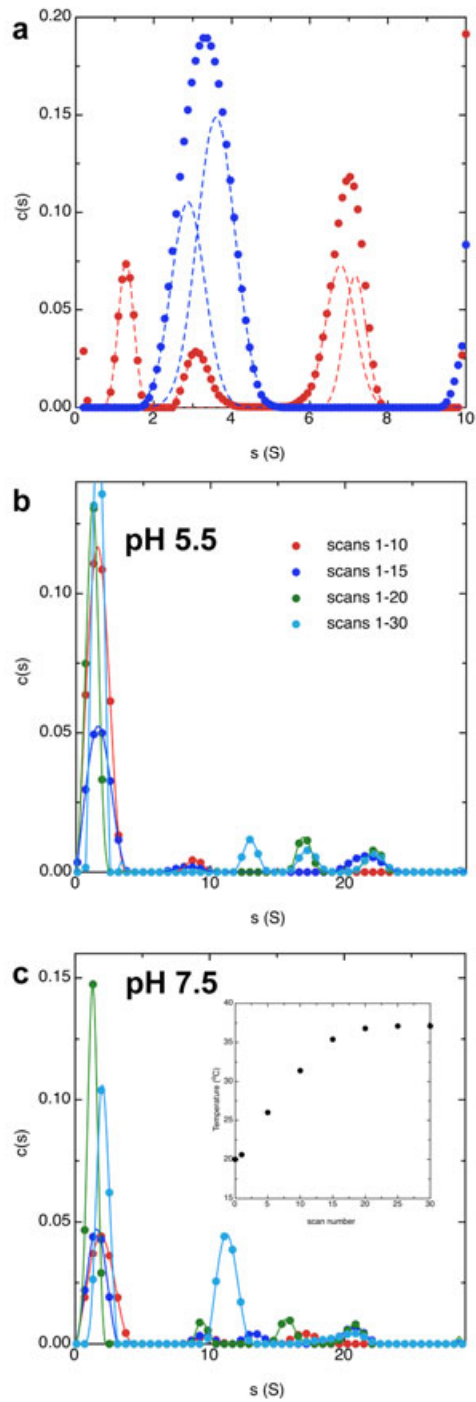


**Figure 2: Analytical ultracentrifugation of LLO**

(a) *Left*  $c(s)$  plots of the apparent sedimentation coefficient distribution for LLO at pH 5.5 (red symbols/fits) and pH 7.5 (blue). 3-4 species are found at pH 5.5 with values of  $s = 1.29 \pm 0.003$ ,  $3.12 \pm 0.01$ ,  $6.79 \pm 0.21$  and  $7.16 \pm 0.05$  S. 1-2 species are found at pH 7.5 with values of  $s =$

$2.88 \pm 0.04$  and  $3.60 \pm 0.04$  S. *Right*  $c(s, M)$  plots of LLO at  $20^\circ\text{C}$  and pH 5.5 (top) and 7.5 (bottom). The plots are temperature coded with red indicating a high probability of a species with such a  $M(s)$  and blue a low probability. Thus for pH 5.5 species between 20 kDa and ~100 kDa are indicated and for pH 7.5 a species of ~70 kDa is indicated. (b) and (c)  $c(s)$  plots for pH 5.5 (b) and pH 7.5 (c) on a rising temperature gradient. The gradient is depicted inset in panel c and the data range used to compute the  $c(s)$  of each colour inset in panel b.

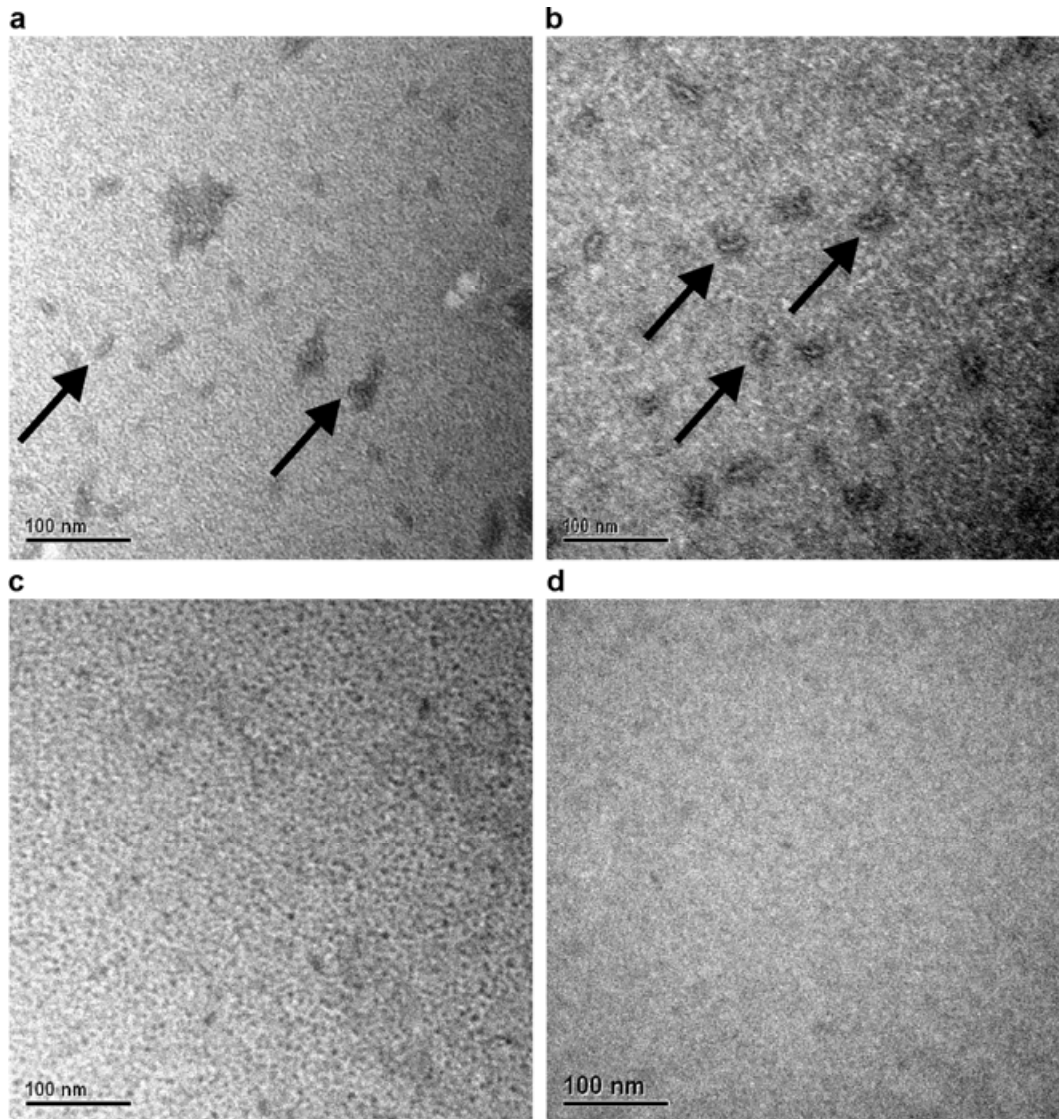


**Figure 3: TEM microscopy of LLO in solution**

(a) LLO at pH 5.5. (b) LLO at pH 5.5 preincubated at 37 °C for 30 min. Slightly curved particles visible at pH 5.5 are denoted by arrows. (c) LLO at pH 7.5. (d) Grid processed in the same way as in a-c but without LLO.

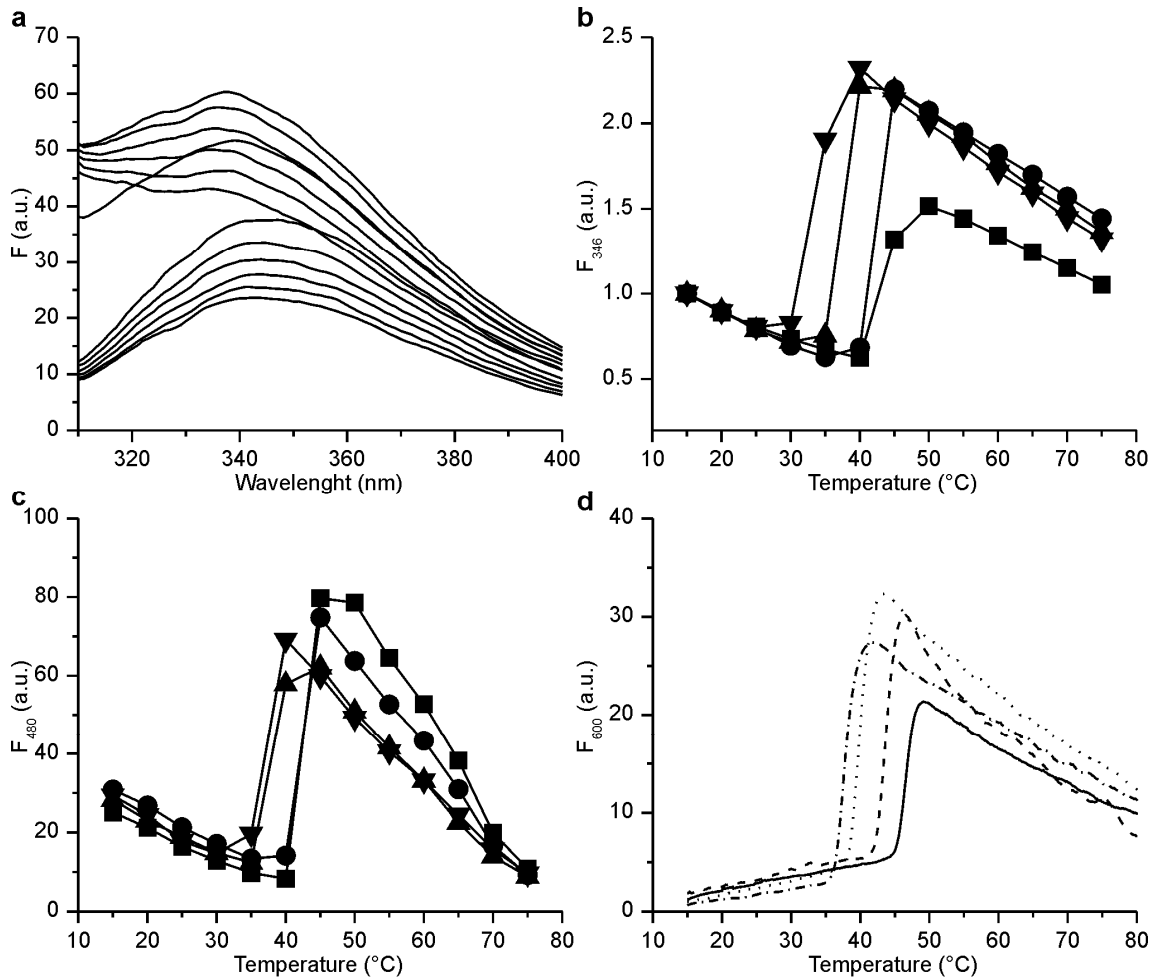


**Figure 4: LLO denaturation induced by increase in temperature**

(a) Trp spectra of 250 nM LLO at different temperatures at pH 5.5. Some of the temperatures are designated. (b) Changes in Trp fluorescence induced by the raise of temperature at different pH values. Squares, pH 5.5; circles, pH 6.5; up-triangles, pH 7.5; down-triangles, pH 8.5. (c) Changes in ANS fluorescence signal induced by the raise of temperature at different pH values. The designations are as in b. (d) Changes in light scattering induced by the raise of temperature at different pH values. Solid line, pH 5.5; dashed line, pH 6.5, dotted line, pH 7.5; dash-dotted line, pH 8.5.

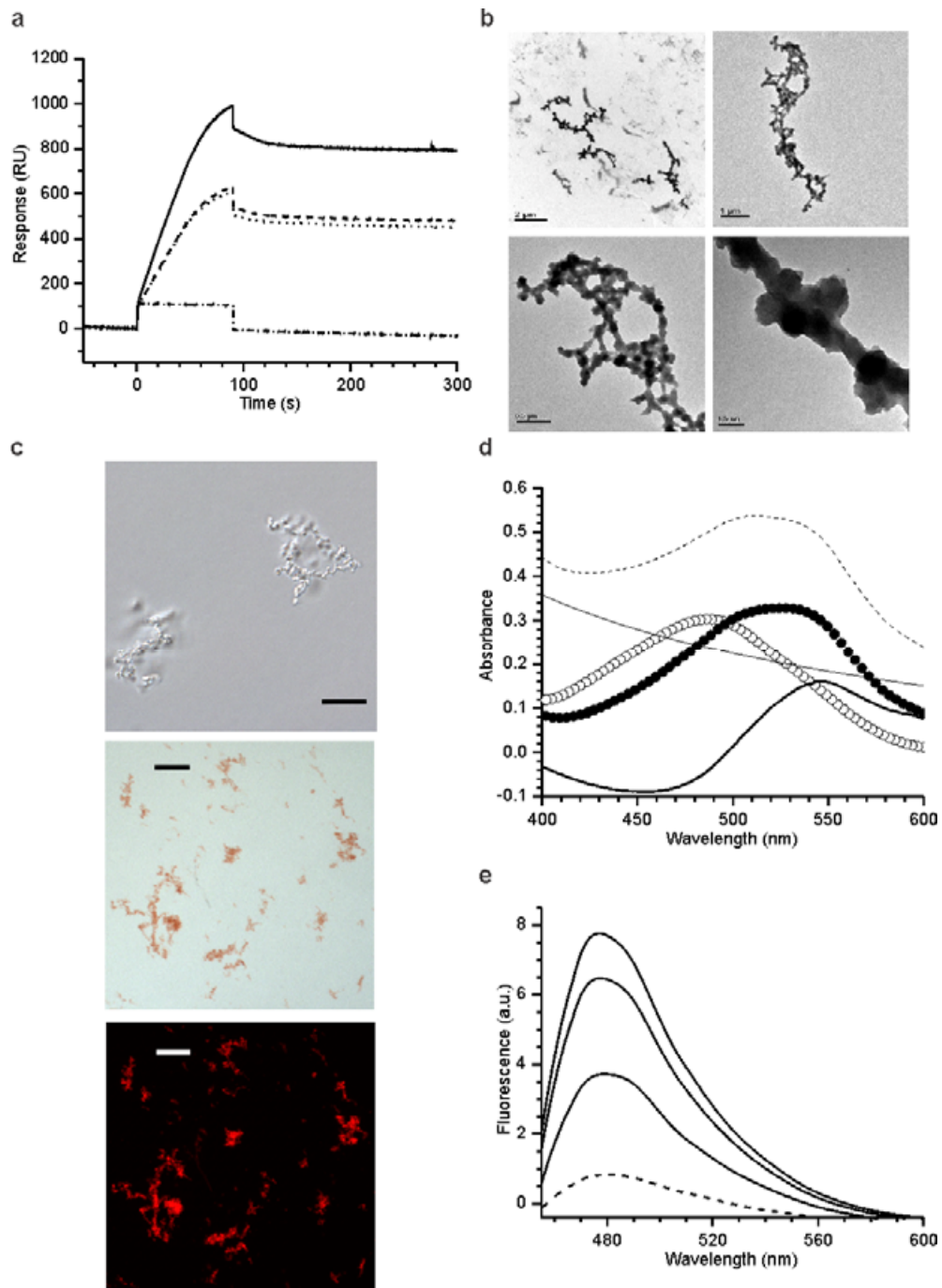


**Figure 5: Properties of aggregates formed by LLO**

(a) SPR analysis of LLO binding after preincubation for 30 min at pH 5.5 and 4 °C (solid line) or 37 °C (dashed line) or at pH 7.5. and 4 °C (dotted line) or 37 °C (dash-dotted line). LUV composed of DOPC:cholesterol 3:2 (mol:mol) were immobilised on L1 sensor chip to saturation and then LLO solutions were injected across the chip for 90 s. (b) TEM analysis of

aggregates formed by LLO at pH 7.5 and exposure to 37 °C. (c) Bright-field and fluorescence microscopy images of aggregates prepared as in b. The scale bar is 10  $\mu\text{M}$  for the upper panel and 50  $\mu\text{M}$  for the bottom two panels. (d) Congo red absorption spectra in the absence (open circles) or in the presence of 2  $\mu\text{M}$  aggregated LLO at pH 7.5 and 37 °C (thin dashed line). The spectrum of aggregated LLO in the absence of Congo red (thin solid line) was subtracted to obtain the corrected Congo red spectrum in the presence of aggregated protein (solid circles). The thick solid line shows the difference between the spectra of Congo red in the presence and absence of aggregated LLO. (e) Fluorescence emission spectra of 20  $\mu\text{M}$  Thioflavin T at 25 °C and pH 7.5 in the presence of 2.5  $\mu\text{M}$  LLO and after temperature was raised to 37 °C and incubated for 5, 10 and 15 min (thick lines from bottom to top).

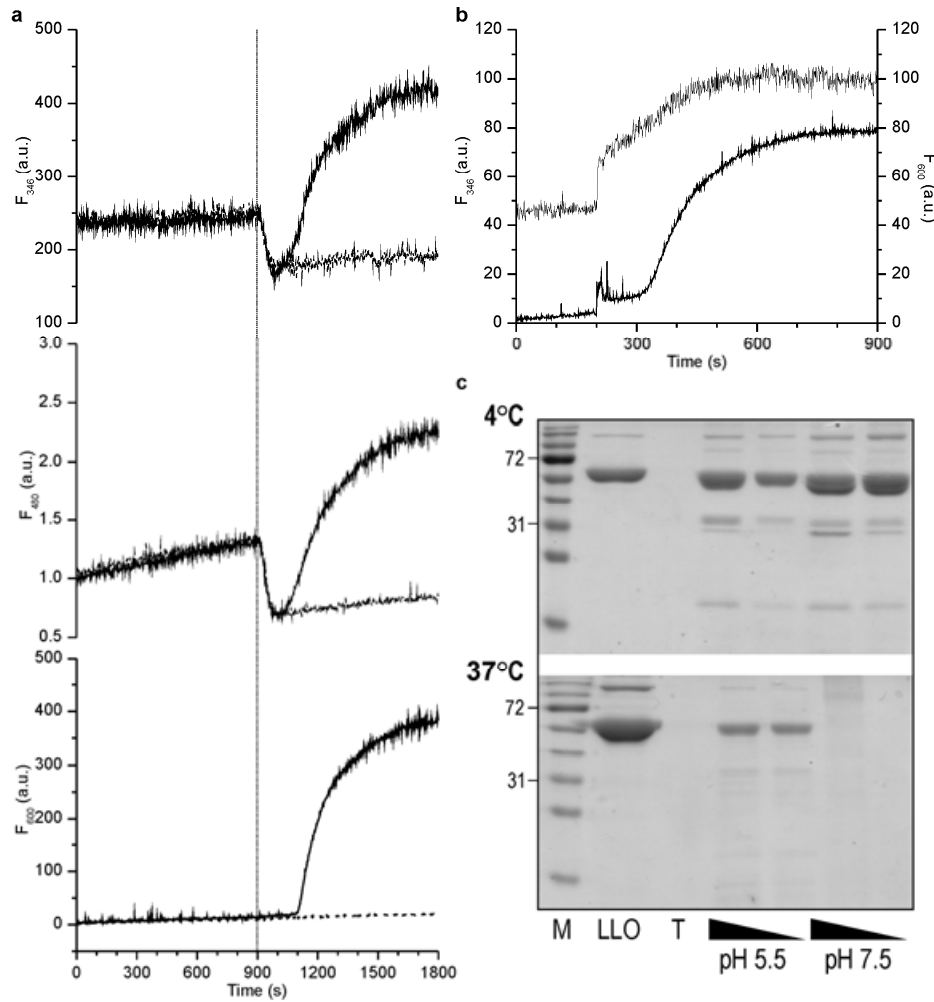


**Figure 6: Kinetics of aggregation of LLO and its stability**

(a) Kinetics of aggregation followed by Trp fluorescence (top), ANS fluorescence (middle) and light scattering (bottom) triggered by the temperature jump from 15 to 37 °C at 900 s, time point indicated by the dashed vertical line. 1  $\mu$ M LLO was kept at pH 5.5 (solid line) or 7.5 (dashed line). (b) Kinetics of LLO aggregation at 27 °C followed by Trp fluorescence (top trace) or light scattering (bottom trace) after change of pH from 5.5 to 7.5 by addition of NaOH at 200 s. Concentration of LLO was 250 nM. (c) Trypsin cleavage assay of LLO preincubated for 60 min at 4 or 37 °C as indicated beside the gels. M, molecular weight marker with masses indicate in kDa. The same marker was used in Figure 1b; LLO, 5  $\mu$ g of LLO; T, 0.083  $\mu$ g of trypsin. LLO was preincubated at pH 5.5 or 7.5 as indicated. Two different amounts of trypsin were used for each pH (0.083 and 0.5  $\mu$ g).

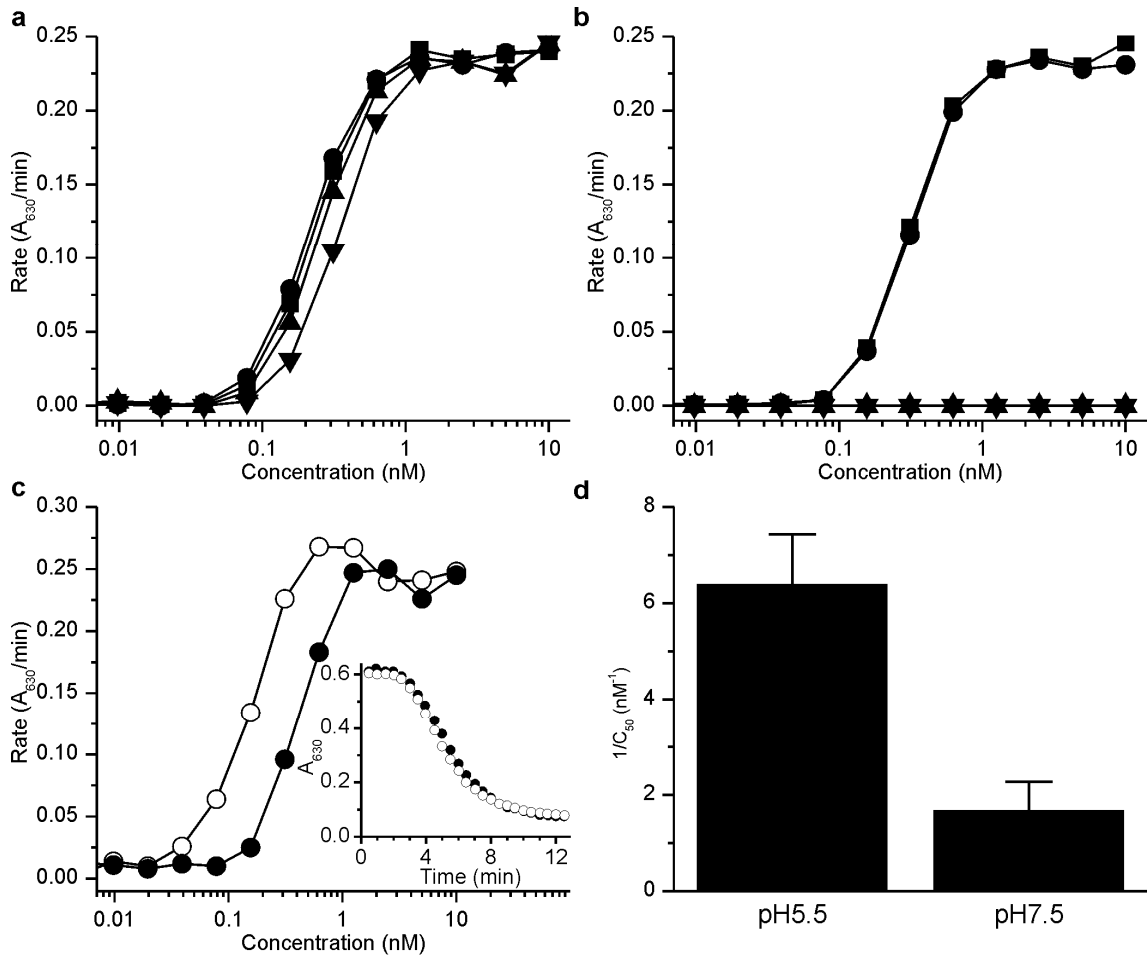


**Figure 7: Hemolysis induced by LLO**

LLO was preincubated for 30 min at different temperatures at pH 5.5 (a) or 7.5 (b) and then immediately assayed for hemolytic activity on human red blood cells at pH 7.5. Squares, 4 °C; circles, 20 °C; up-triangles, 37 °C; down-triangles, 42 °C. (c) Hemolysis of human red blood cells induced by various concentrations of LLO assayed at pH 5.5 (open circles) or 7.5 (solid circles) at room temperature. The inset shows the time course of hemolysis induced by approximately 150 pM LLO at pH 5.5 (open circles) or 625 pM LLO at pH 7.5 (solid circles). (d) 1/C<sub>50</sub> values determined from the data presented on panel c. n=4, average±S.D.

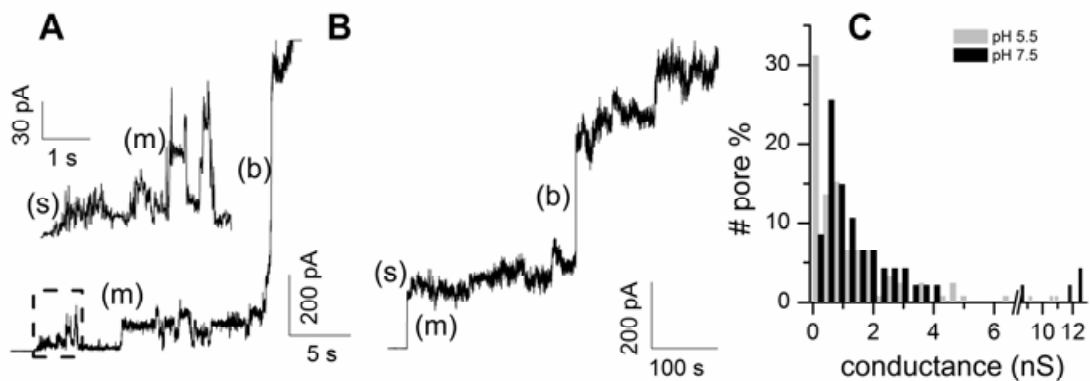


**Figure 8: Planar lipid bilayer experiments**

(a) Current steps after addition of LLO 10 nM to one side of DOPC:cholesterol 80:20 (mol:mol) planar bilayer clamped at +40mV. Experiment was carried out in KCl 100 mM and MES 10 mM pH 5.5 at 24°C. In this recording small (s) and medium (m) pores (0.5 ÷ 2 nS) are followed by bigger (b) ones (3.0, 10.6 nS). Then other pores respectively of 0.8, 1.0 and 12.0 nS are evident. Finally, the membrane brakes. (b) In this trace first a big pore (4 nS) appears followed by some small ones (0.5, 0.6, 0.7 nS), medium (1.9 nS) and finally a big one (8.7 nS). Experimental condition: KCl 0.1 M Hepes 10 mM pH 7.5. Planar bilayer was comprised of DOPC:cholesterol 65:35 (mol:mol). (c) Histogram of LLO conductance events distribution. Events are detected from 25 different experiments (a total of 125 pores at pH 5.5 and 48 pores at pH 7.5). The conductivity is very spread at both pHs and no pore size difference exists between the two pH conditions. No pore size difference are present either at different cholesterol content (20% or 35%).